SUPPORTING INFORMATION

Theoretical study of the electrochemical reduction of CO_2 on cerium dioxide supported palladium single atoms and nanoparticles

Yannv Guo,[a] Haiyan Zhu,[a] He Zhao,[a] Qinfu Zhao,[a] Caihua Zhou,[b] Bingbing Suo,[a]*

Wenli Zou,[a] Zhenyi Jiang,[a] and Yawei Li[a]*

[a] Shaanxi Key Laboratory for Theoretical Physics Frontiers, Institute of Modern Physics, Northwest University, Xi'an, Shaanxi 710069, China

[b] School of Chemistry and Chemical Engineering, Xianyang Normal University, Xianyang, Shaanxi 712000,China

Corresponding Authors

*E-mail: zhuhaiyan@nwu.edu.cn

*E-mail: yawei.li@epfl.ch

Artificial bee colony algorithm in ABCluster

The AB Cluster procedure[1] uses an artificial bee colony for global search of the cluster, which is an efficient, user-friendly, and free software to perform the global optimization of clusters by the ABC algorithm. The artificial bee colony (ABC) algorithm, which is a swarm intelligence based one, was first proposed by Karaboga in 2005.[2] It was inspired by the foraging behavior of honey bee colonies. In these colonies, bees want to find the best source of nectar. To achieve this goal efficiently, bees are specialized for different tasks. In the model of the ABC algorithm, there are three kinds of bees: employed, onlooker, and scout bees. Each bee can find nectar and estimate its ‘‘quality’’. More importantly, it can share this information with other bees by, e.g., a waggle dance. This communication between individuals is the basis of the colony's random and feedback behavior. During a search cycle, employed bees search for new sources of nectar based on their knowledge as well as that of other bees. The onlooker bees then communicate with the employed bees to search for new nectar sources around "good" nectar sources. Based on feedback from the employed and onlooker bees, the low-quality nectar source is discarded and the scout bees search for a new nectar source. After several cycles, the "best" nectar source is finally selected.

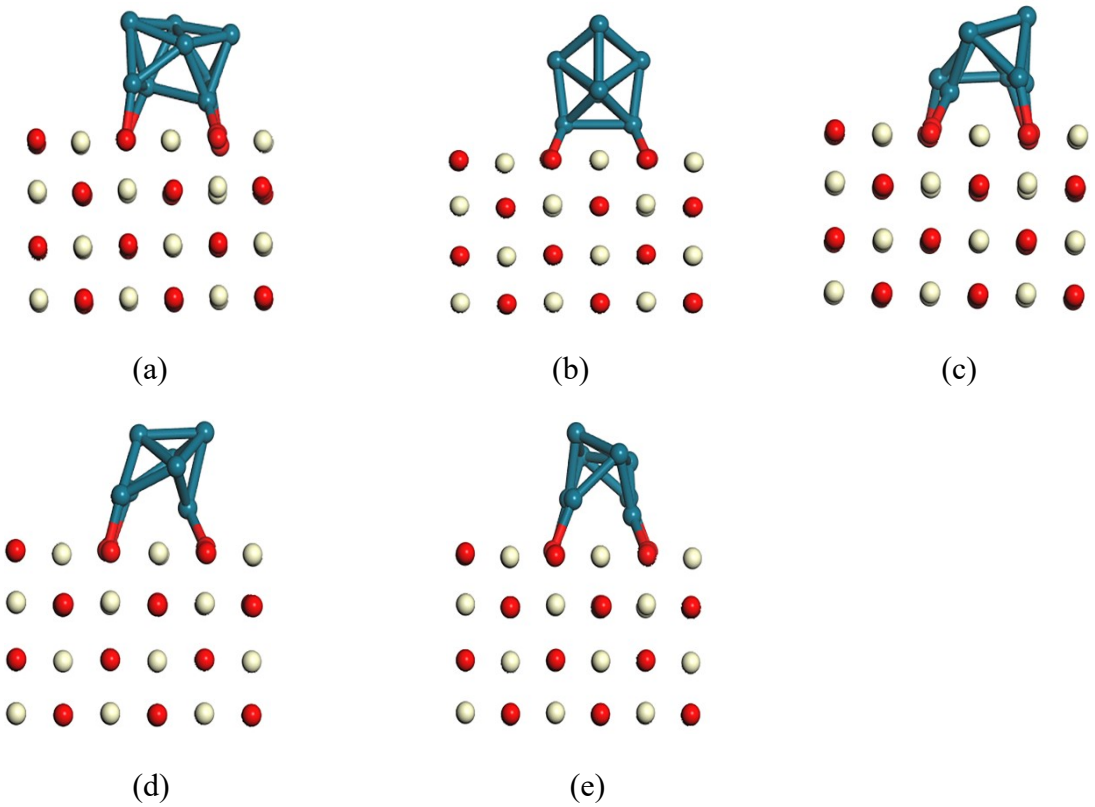

Figure S1. Possible binding structures of Pd_8 clusters deposited on CeO_2 substrates. Red: O atoms; blue : Pd atoms; yellow: Ce atoms;brown:C atoms.

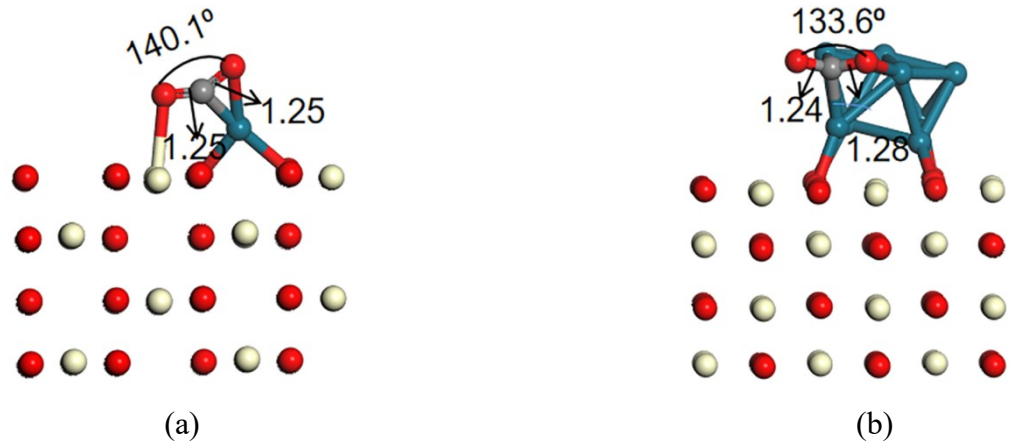

Figure S2. (a) Side view of optimized structure of Pd/CeO_2 for CO_2 adsorption(b)Side view of optimized structure of Pd_8/CeO_2 for CO_2 adsorption. Red: O atoms; blue : Pd atoms; yellow: Ce atoms;brown:C atoms.

Density of states (DOS) analysis of structures for CO_2 adsorption

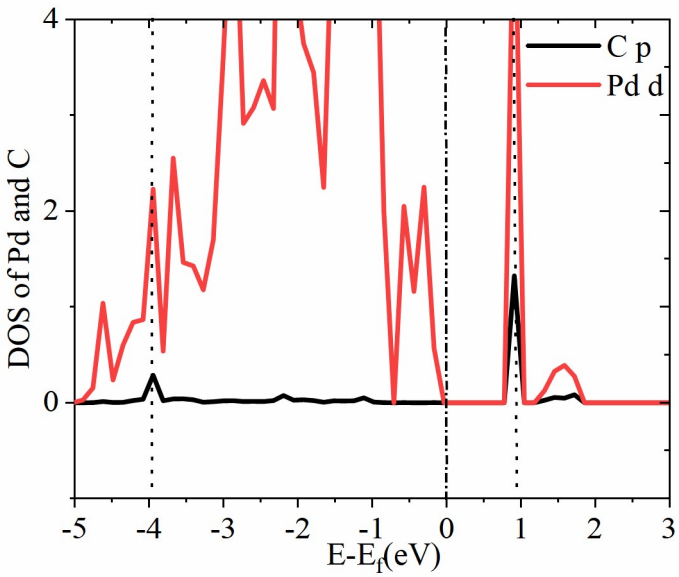

Figure S3. Projected density of states (DOSs) of Pd atom (red line) and C atom (black line) directly involved in bonding with C for structure b in Table 1. The dotted dash line indicates Fermi level; the dashed lines indicate direct overlap between C and Pd.

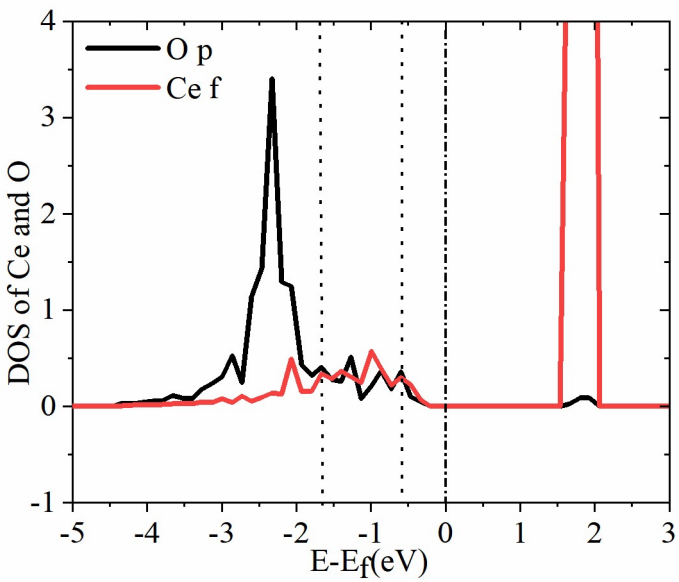

Figure S4. Projected density of states (DOSs) of Ce atom (red line) and O atom (black line) directly involved in bonding with Ce for structure d in Table 1. The dotted dash

line indicates Fermi level; the dashed lines indicate direct overlap between Ce and O.

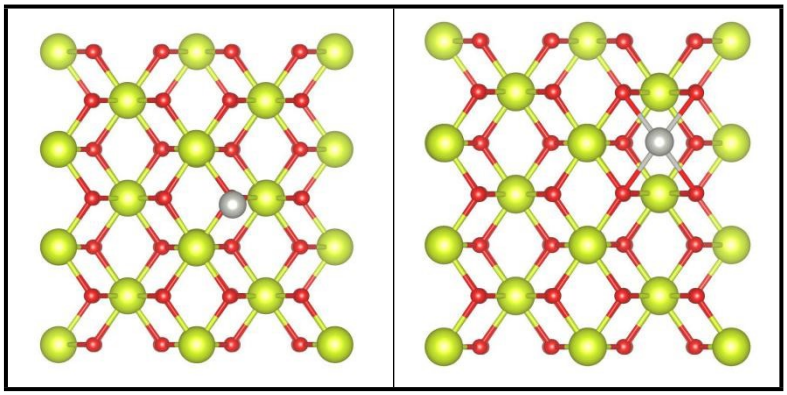

O_T -1.67eV O_H -1.90eV

Table S1. Optimized adsorption configurations and adsorption energies (in eV) on Pd/CeO_2

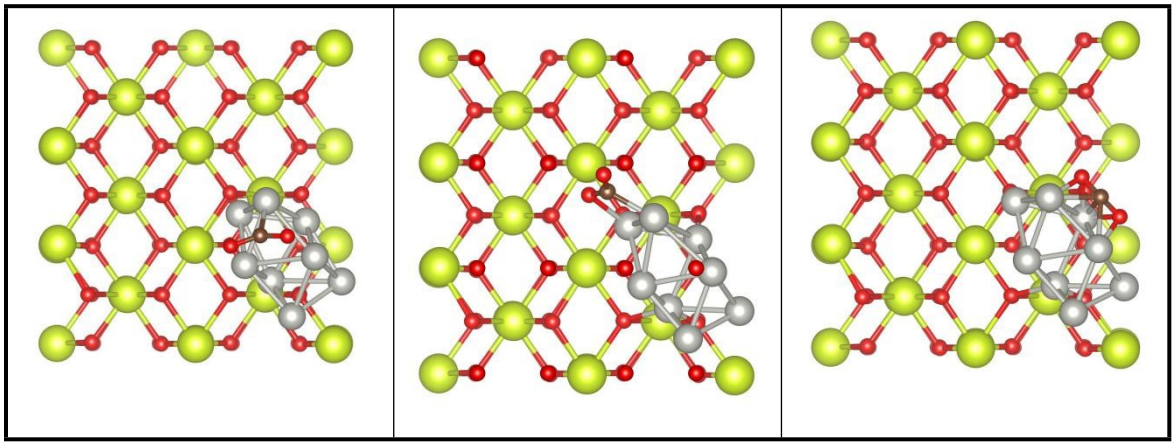

-0.35eV -0.45eV -0.29eV

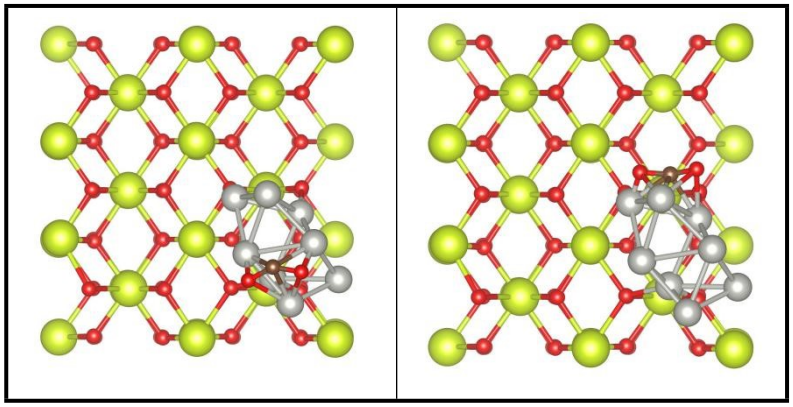

-0.11eV -0.38eV

Table S2. Optimized adsorption configurations and adsorption energies (in eV) of CO_2 on Pd_8/CeO_2

Table S3. Possible reduction steps in the electrochemical reduction of CO_2 on Pd/Pd_8/-CeO_2 and the corresponding reaction free energies (ΔG) at 0 V (vs. RHE)

Elementary steps	ΔG(eV)	
	Pd_8/CeO_2	**Pd/CeO_2**
$CO_2 + * \rightarrow *CO_2$	-0.08	-0.98
$*CO_2 + H^+ + e^- \rightarrow *COOH$	0.07	0.8
$*CO_2 + H^+ + e^- \rightarrow *OCHO$	0.02	0.3
$*COOH + H^+ + e^- \rightarrow *CO + H_2O$	-1.35	-1.26
$*COOH + H^+ + e^- \rightarrow *HCOOH$	0.09	0.6
$*OCHO + H^+ + e^- \rightarrow *HCOOH$	0.14	1.10
$*HCOOH \rightarrow * + HCOOH$	0.3	-0.04
$*OCHO + H^+ + e^- \rightarrow *H_2COO$	1.47	1.16
$*H_2COO + H^+ + e^- \rightarrow *H_2COOH$	-0.66	-0.23
$*CO + H^+ + e^- \rightarrow *CHO$	1.19	1.6
$*HCOOH + H^+ + e^- \rightarrow *CHO + H_2O$	-0.24	-0.26
$*HCOOH + H^+ + e^- \rightarrow *H_2COOH$	0.67	-0.17
$*H_2COOH + H^+ + e^- \rightarrow *OCH_3 + *OH$	-0.51	-1.58
$*H_2COOH + H^+ + e^- \rightarrow *OCH_2 + H_2O$	-0.76	-1.05
$*H_2COOH + H^+ + e^- \rightarrow CH_3OH + *O$	0.01	1.61
$*OCH_3 + *OH + H^+ + e^- \rightarrow CH_4 + *O + *OH$	-0.51	0.71
$*O + *OH + H^+ + e^- \rightarrow 2*OH$	-0.87	-1.93
$2*OH + H^+ + e^- \rightarrow *OH + H_2O$	0.03	0.93
$*OCH_3 + *OH + H^+ + e^- \rightarrow CH_3OH + *OH$	-0.11	0.95
$*OCH_3 + *OH + H^+ + e^- \rightarrow *OCH_3 + H_2O$	0.29	1.52
$*CO + H^+ + e^- \rightarrow *COH$	2.72	2.74
$*COH + H^+ + e^- \rightarrow *C + H_2O$	1.08	1.39
$*CHO + H^+ + e^- \rightarrow *CH_2O$	0.15	-0.96
$*CHO + H^+ + e^- \rightarrow *CHOH$	1.09	0.15
$*CH_2O + H^+ + e^- \rightarrow *OCH_3$	0.54	0.99
$*CH_2O + H^+ + e^- \rightarrow *CH_2OH$	0.05	1.17
$*CHOH + H^+ + e^- \rightarrow *CH_2OH$	-0.9	0.06

$*CHOH + H^+ + e^- \rightarrow *CH + H_2O$	-1.19	1.33
$*OCH_3 + H^+ + e^- \rightarrow CH_3OH + *$	-0.57	-0.23
$*OCH_3 + H^+ + e^- \rightarrow *O + CH_4$	-1.02	0.43
$*CH_2OH + H^+ + e^- \rightarrow CH_3OH + *$	-0.15	-0.41
$*CH_2OH + H^+ + e^- \rightarrow *CH_2 + H_2O$	-0.03	-0.37
$*C + H^+ + e^- \rightarrow *CH$	-2.7	-1.06
$*CH + H^+ + e^- \rightarrow *CH_2$	-0.21	-1.64
$*CH_2 + H^+ + e^- \rightarrow *CH_3$	-0.35	-0.71
$*CH_3 + H^+ + e^- \rightarrow CH_4 + *$	-0.47	-0.57
$*O + H^+ + e^- \rightarrow *OH$	-0.62	-2.24
$*OH + H^+ + e^- \rightarrow H_2O + *$	-0.17	0.34

Table S4. The energy corrections of free molecules discussed

Free molecules	**G(eV)**	**E_{ele}(eV)**	**ZPE(eV)**	**TS(eV)**
CO_2(g)	-23.24	-22.975	0.306	0.566
H_2(g)	-6.808	-6.758	0.266	0.316
CO(g)	-15.18	-14.79	0.131	0.521
H_2O(l)	-14.22	-14.22	0.566	0.568
HCOOH(g)	-29.663	-29.893	0.883	0.653
CH_4(g)	23.31	-24.03	1.189	0.469
CH_3OH(l)	-29.48	-30.21	1.354	0.624

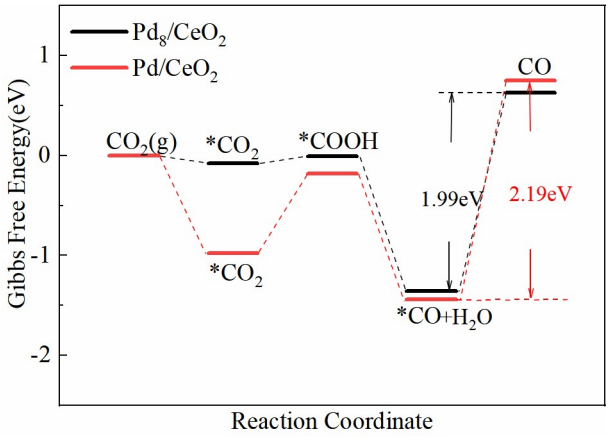

Figure S5. Gibbs Free energy diagram for CO production of CRR on Pd_8/CeO_2 and Pd/CeO_2 (at 0V vs reversible hydrogen electrode).

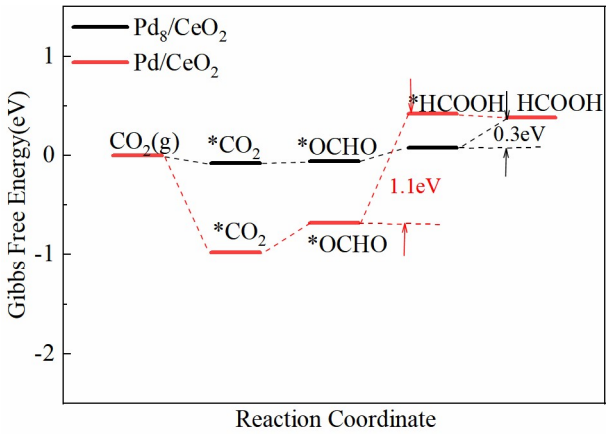

Figure S6. Gibbs Free energy diagram for HCOOH production of CRR on Pd_8/CeO_2 and Pd/CeO_2 (at 0V vs reversible hydrogen electrode).

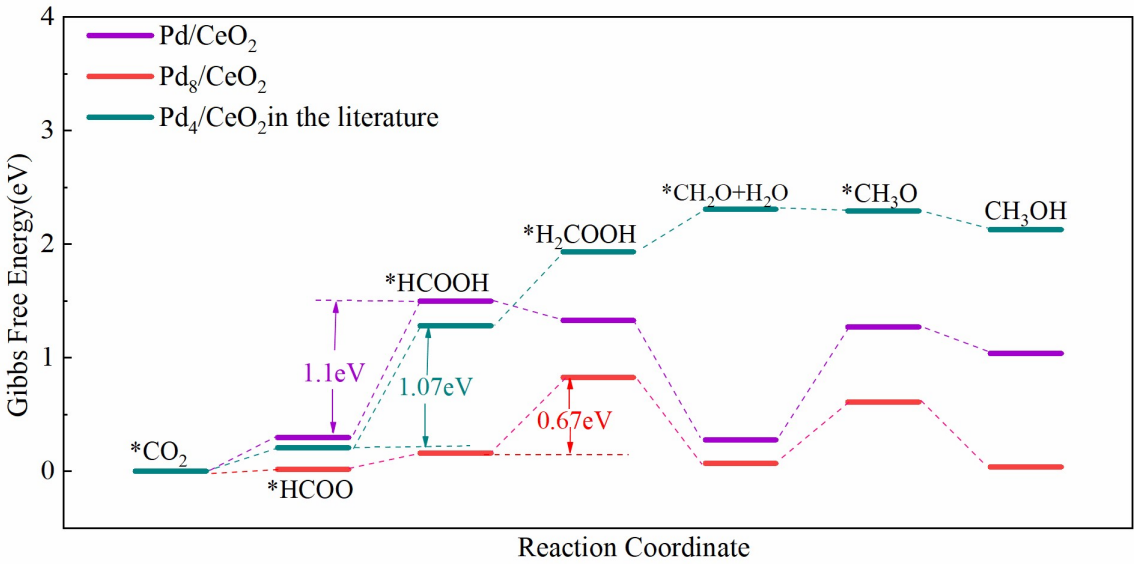

Figure S7. Free energy curves of CH_3OH production by CRR on Pd/CeO_2, Pd_8/CeO_2, and Pd_4/CeO_2 (0 V vs. reversible hydrogen electrode) in the literature.

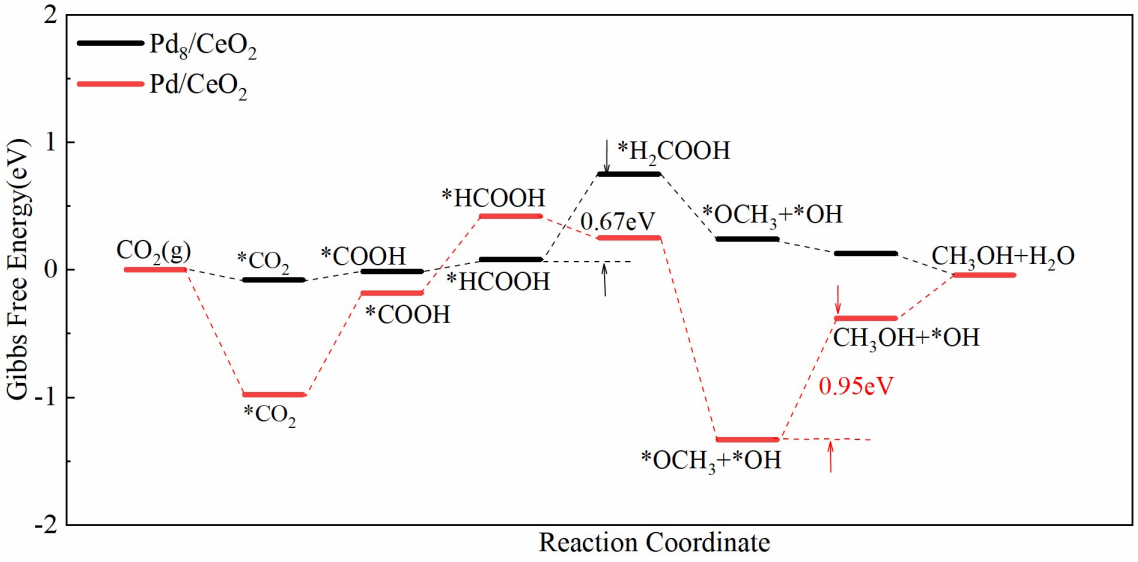

Figure S8. Gibbs Free energy diagram for CH_3OH production of CRR on Pd_8/CeO_2 and Pd/CeO_2 (at 0V vs reversible hydrogen electrode).

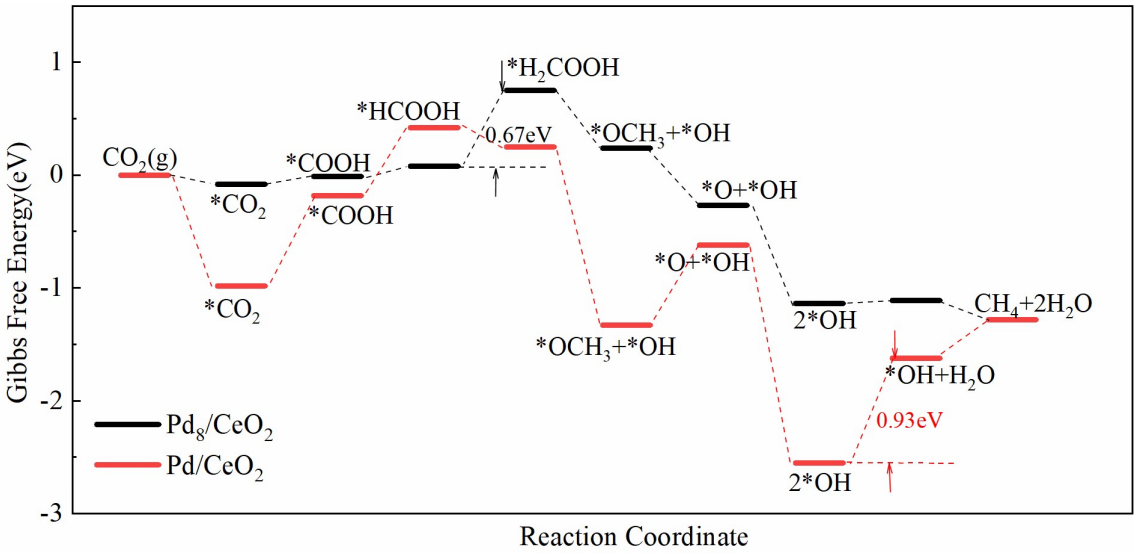

Figure S9. Gibbs Free energy diagram for CH_4 production of CRR on Pd_8/CeO_2 and Pd/CeO_2 (at 0V vs reversible hydrogen electrode).

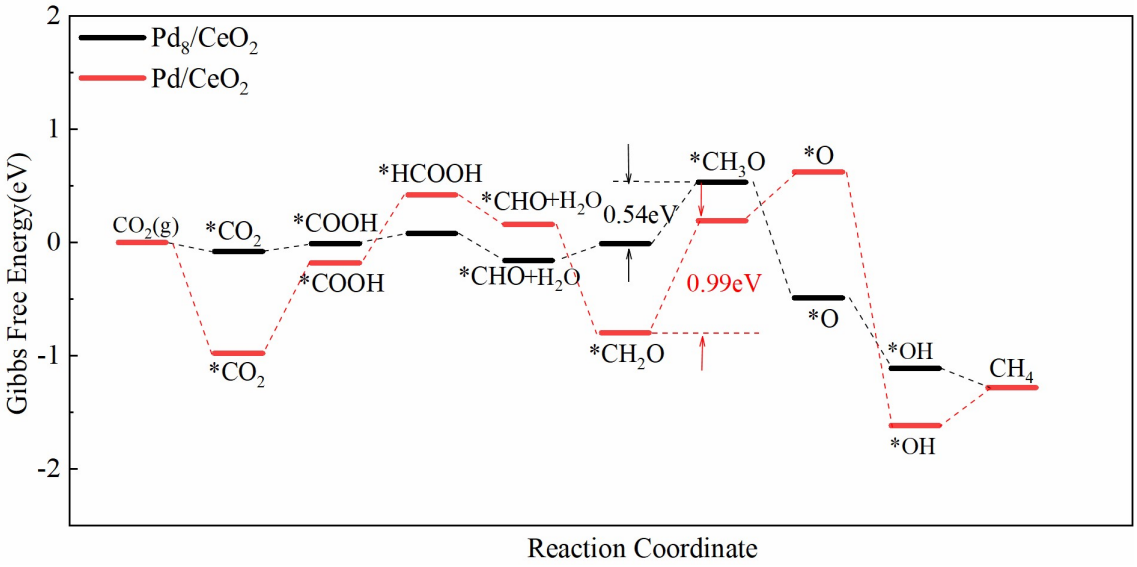

Figure S10. Gibbs Free energy diagram for CH_4 production of CRR on Pd_8/CeO_2 and Pd/CeO_2 (at 0V vs reversible hydrogen electrode).

Reference

(1) J. Zhang, M. Dolg, *Physical chemistry chemical physics:PCCP,* 2015, **17**, 24173-24181.

(2) D. Karaboga, *Computer Science,* 2005.